Band structure and Fermi surface of $TmGa_3$

V. B. Pluzhnikov
International Laboratory of High Magnetic Fields and Low Temperatures, Gajowicka 95, 53-529 Wrocław, Poland and B. Verkin Institute for Low Temperature Physics and Engineering, 47 Lenin Prosp., Khar'kov 310164, Ukraine

A. Czopnik*
W. Trzebiatowski Institute of Low Temperature and Structure Research, P.O. Box 1410, 50-950 Wrocław, Poland

G. E. Grechnev and N. V. Savchenko
B. Verkin Institute for Low Temperature Physics and Engineering, 47 Lenin Prosp., Khar'kov 310164, Ukraine

W. Suski
International Laboratory of High Magnetic Fields and Low Temperatures, Gajowicka 95, 53-529 Wrocław, Poland and W. Trzebiatowski Institute of Low Temperature and Structure Research, P.O. Box 1410, 50-950 Wrocław, Poland

(Received 23 January 1998; revised manuscript received 4 September 1998)

In the present work the Fermi surface geometry and cyclotron masses of a $TmGa_3$ antiferromagnet in a field-induced paramagnetic phase are determined by using the de Haas–van Alphen–effect method. The results are analyzed on the basis of *ab initio* band structure calculations for $TmGa_3$ and $LuGa_3$. [S0163-1829(99)03611-5]

I. INTRODUCTION

In the present work we continue our recent[1] studies on the electronic structure of the cubic R_EGa_3 (R_E denotes heavy rare-earth metal) compounds. The aim of the work is the determination of the Fermi surface (FS) geometry and effective cyclotron masses of $TmGa_3$ by means of the de Haas–van Alphen (dHvA) effect. The results are analyzed on the basis of self-consistent band structure calculations of $TmGa_3$ and $LuGa_3$ compounds.

$TmGa_3$ crystallizes in the cubic $AuCu_3$-type structure with the lattice constant $a=4.196$ Å . At 4.26 K it undergoes antiferromagnetic transition[2] to the multiaxial 3**k**-type structure.[3,4] In the paramagnetic state an interaction between quadrupolar moments of the $4f$ shells is so strong that it leads to their ordering just above T_N; it has been shown that the leading mechanism is pair quadrupolar interaction by conduction electrons.[5]

In Fig. 1 the magnetic phase diagram in magnetic field parallel to the $\langle 001\rangle$ axis is shown (cited from Ref. 4). The antiferroquadrupolar phase exists only in low fields up to 0.5 T and in the very narrow range of temperatures $(T_Q, T_N) < 0.1$ K. The critical lines $H_{c_1}(T)$ and $H_{c_2}(T)$ are the lines of metamagnetic transitions: in the field $H_{c_1}(T)$ from the 3**k** phase to an intermediate one and in $H_{c_2}(T)$ from the intermediate phase to the paramagnetic one.

In the field applied along the other two principal crystallographic axes, $\langle 110\rangle$ and $\langle 111\rangle$, the diagrams are similar to the one cited but the critical field $H_{c_2}(T)$ reaches much lower values and does not exceed 2.2 T. At temperatures lower than T_N and in magnetic field higher than 7 T, magnetic moments reach induced paramagnetic configuration, except for the small region of angles around the $\langle 001\rangle$ axis. Above the second metamagnetic transition the magnetization is large and very anisotropic. This fact has important consequences for the dHvA effect analysis.

First, in the Fourier analysis of the detected dHvA signal v one must take into account the magnetic induction B in the Lifshitz-Kosevich formula instead of the applied magnetic field H_{appl},

$$v \propto A \sin[(2\pi F/B)+\phi],$$

where the magnetic induction $B=H_{\text{appl}}+4\pi M(1-N)$ depends on magnetization per unit volume and on demagnetizing factor N.

Second, the dHvA frequency F is proportional to the extremal FS cross-section area perpendicular to the magnetic induction **B**. However, in the case under consideration, even at the fixed direction of the magnetic field, the direction of

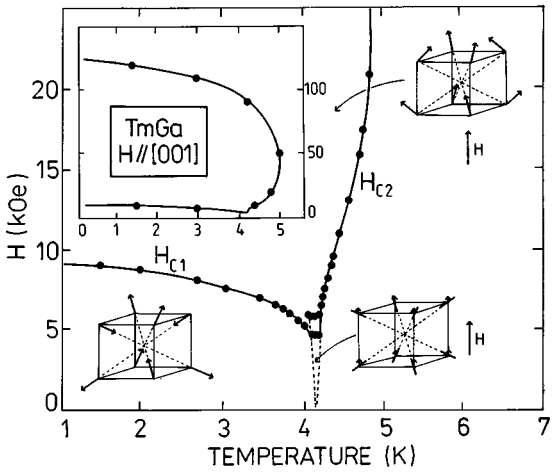

FIG. 1. Low field magnetic phase diagram of $TmGa_3$ for a magnetic field along [001]. The inset shows the whole diagram.

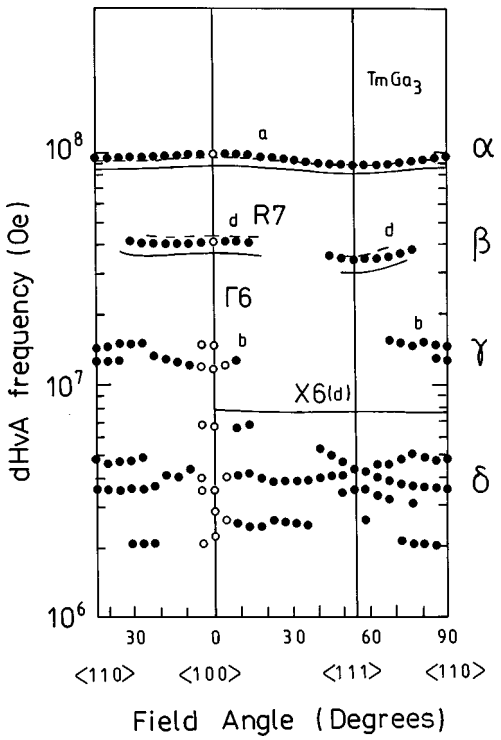

FIG. 2. Angular dependence of the dHvA frequencies in $TmGa_3$: filled circles — in the field higher than the second critical field, empty circles — in the field lower than H_{c2}. Curves show calculated results for spin up (dashed) and spin down (solid).

magnetic induction changes continuously with increasing magnetic field until the magnetization saturates and then $\mathbf{B}\|\mathbf{H}_{\text{appl}}$.

Third, in order to avoid broadening of the phase oscillation, the samples should have an ellipsoidal form. In turn, the necessity of the constancy of the demagnetizing factor N under rotation limits the shape of the samples used to spheres.

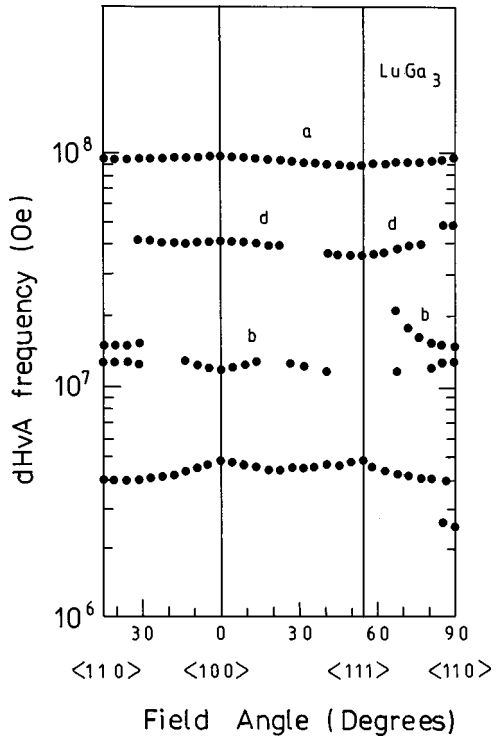

FIG. 3. Angular dependence of the dHvA frequencies in $LuGa_3$ cited from Ref. 1.

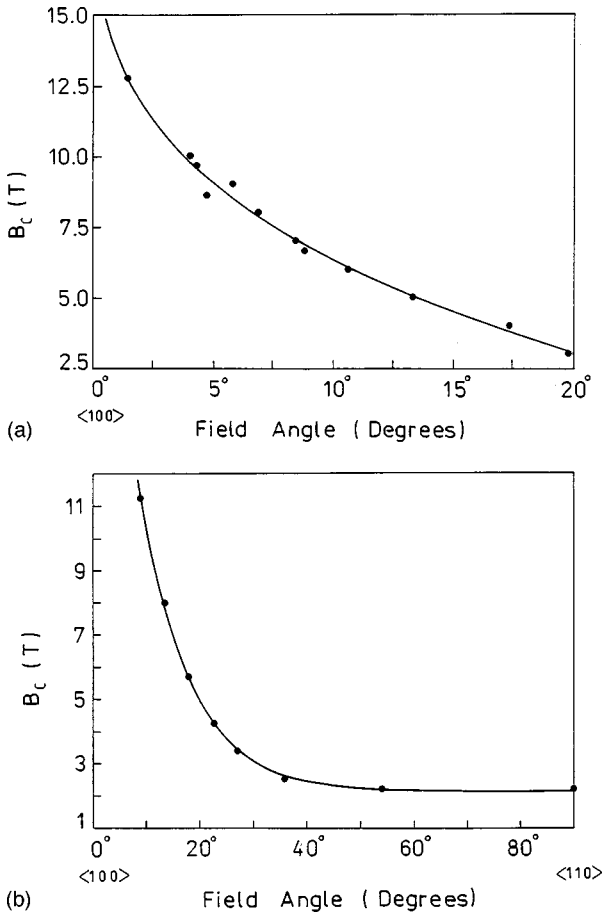

FIG. 4. Angular dependence of the second critical field in the plane (100) (a) and (110) (b) in $TmGa_3$ at $T=2.6$ K.

Fourth, in a strong magnetic field the magnetic moments of Tm^{3+} ions reach spin-polarized paramagnetic configuration. Then the k-f exchange interaction leads to a splitting of the conduction band into subbands with spins parallel and antiparallel to the direction of the magnetic induction. The value of the band splitting should be proportional to the magnetic moment value and the k-f exchange integral.

The next complication which one may expect comes from the fact that the ground state $^3H_6$ of Tm^{3+} ions in the crystal field (CF) of $TmGa_3$ is the triplet $\Gamma_5^{(1)}$.[3] This state is characterized, in addition to the magnetic dipole moment, by the electric quadrupole one. In an applied magnetic field the quadrupolar moments follow the rotation of magnetic moments. The rotation of quadrupoles leads to (1) a change of interatomic distances and (2) a perturbation of the cubic symmetry. Therefore, the rotation of the quadrupoles is equivalent to applying uniaxial stress with magnitude and direction depending on the strength and the direction of magnetic field. The symmetry changes that follow may remove degeneracy of FS at points of self-crossing. A change of the interatomic distances may lead to a topological transition, i.e., appearance of the new sheets of FS.

TABLE I. dHvA frequencies and the corresponding cyclotron masses in $TmGa_3$.

⟨001⟩		⟨110⟩		⟨111⟩	
$F(10^6$ Oe)	m_c/m_0	$F(10^6$ Oe)	m_c/m_0	$F(10^6$ Oe)	m_c/m_0
2.25		2.02			
2.89					
3.58		3.57	0.46	3.55	
6.65		4.80		4.31	0.50
11.69	0.82	12.66	0.96		
14.79		14.60			
41.08	1.47(1.3) [a]			34.24	0.90
98.70	1.40(1.2) [a]	94.41	1.02 ± 0.03 [b]	87.28	0.77

[a]Measurement below the second critical magnetic field.

[b]Accuracy of all other measurements of m_c/m_0 is equal to ±0.01.

II. EXPERIMENT

The single crystal species of investigated compounds were prepared by the slow cooling method (0.6–0.8 K/h) of the alloy composed of 90 at. % Ga and 10 at. % Tm or Lu in the resistance furnace. The synthesis was carried out in the alundum crucible located in a quartz ampoule in argon atmosphere under pressure of 150 torr at room temperature. To obtain sufficiently large single crystals the process of a few slow thermal cycles in a range below the liquidus-solidus line for selecting only the largest seeds is applied. The synthesis was stopped at about 300 °C and then the sample was quickly cooled to room temperature in order to avoid the formation of R_EGa_6 compounds in peritectic reaction.[6] The purity of starting metals was $6N$ for Ga and $3N$ for Tm and Lu. The resulting crystals of the R_EGa_3 compounds were immersed in an excess of Ga which is easy to remove. The largest single crystals have dimensions $6\times6\times5$ mm^3. According to the x-ray examination the quality of the samples is very good.

The dHvA-effect measurements were performed on a spherical sample (diameter 2.5 mm) by using the standard field modulation method at temperatures down to 1.5 K and in magnetic fields up to 13 T. In order to investigate the angular dependence of the dHvA frequencies the sample could be rotated. This allowed us to carry out the measurements in the field in the (100) and (110) planes. The dHvA-effect measurements were carried out in the paramagnetic phase well above the $H_c(T)$ line of the antiferromagnetic-paramagnetic transition (Fig. 1), except for a small angle region around the ⟨001⟩ axis, for which the critical field reaches significant values [Fig. 4(a)].

For this intensity range the magnetic field induces a paramagnetic (or quasiferromagnetic) configuration of magnetic moments (not a ferromagnetic state). When this configuration is attained, the magnetization does not change distinctly and it is possible to analyze dHvA frequencies. In the other case dHvA frequencies would change in value following the strength of the external magnetic field. Also, in the field-induced quasiferromagnetic configuration the dHvA spectrum for $TmGa_3$ can be compared with the results of the band structure calculations for the spin-polarized state.

The effects resulting from the influence of antiferromagnetic and antiferroquadrupolar order on the Fermi surface have not been examined in this research. For these phases the large magnetization value and its strong dependence on magnetic field have not allowed us to analyze the dHvA oscillations. Also, a very narrow temperature range (<0.1 K) for the antiferroquadrupolar phase has prevented a corresponding study of the dHvA effect.

III. RESULTS

The angular dependencies of the dHvA frequencies in the (100) and (110) planes for $TmGa_3$ are shown in Fig. 2. The corresponding dHvA frequencies and cyclotron masses along principal crystallographic axes, ⟨100⟩, ⟨110⟩, and ⟨111⟩, are given in Table I. For comparison and further discussion, the angular dependencies of the dHvA frequencies taken from Ref. 1 for $LuGa_3$ are shown in Fig. 3.

The Fourier analysis of the dHvA oscillations was performed by taking into account the magnetic induction $\mathbf{B}=\mathbf{H}_{\mathrm{appl}}+(8\pi/3)\mathbf{M}$. Magnetization in magnetic fields, used for dHvA-effect measurement, depends rather weakly on the magnetic field strength. For the analysis we have employed magnetization data up to 7 T from Ref. 4. Also, we used our supplementary magnetization measurement data for the fields above 7 T.

In order to find the field dependence of magnetization in other directions than along principal crystallographic axes, we have applied the following procedure. In the molecular-field approximation we have calculated magnetization self-consistently. The Hamiltonian employed contains the crystal field, and the exchange and Zeeman terms. The values of the interaction parameters were taken from Refs. 3–5. The calculated values of the magnetization differ by about 25% from the experimental ones, but the character of the field dependence is very similar. We assumed, therefore, that the calculations have given correct angular dependencies of the magnetization at the constant fields. The attempts to improve agreement between the experimental and calculated magnetizations by including the magnetoelastic and quadrupolar terms to the Hamiltonian have failed. Therefore, the calculated values of the magnetization, normalized to the experimental ones along the principal crystallographic axes, were used in the Fourier analysis of dHvA oscillations.

The second important assumption, which we made to get parameters for the Fourier analysis, was that the magnetization vector is parallel to the magnetic field vector. This as-

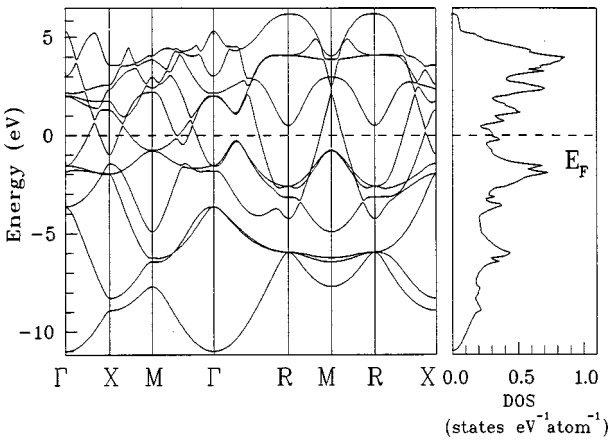

FIG. 5. Energy band structure along high symmetry lines and total density of states calculated for $LuGa_3$ by LMTO method. The energy is measured from the Fermi energy E_F.

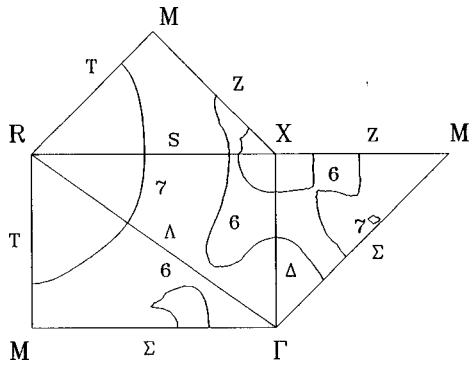

FIG. 6. Intersection of FS for $LuGa_3$ with high symmetry planes. ''6'' and ''7'' — zone numbers.

sumption may be accepted because for nearly all directions the applied magnetic field was large enough to reach the quasiferromagnetic configuration. Only along the ⟨100⟩ axis and at angles close to it was the critical magnetic field, above which magnetic moments reach the quasiferromagnetic configuration, so high that the dHvA-effect measurements were performed in fields below the critical value.

The angular dependencies of the dHvA frequencies were measured at 2.6 K and at the same temperature we determined in the (100) and (110) planes the angular dependence of the critical magnetic field which leads to the quasiferromagnetic configuration. The results are shown in Figs. 4(a) and 4(b). Very strong increase of the critical magnetic field is seen when one approaches the ⟨100⟩ axis.

Upon comparing the angular dependencies of the extremal cross-section area of FS for $TmGa_3$ and $LuGa_3$ (Figs. 2 and 3) it is seen that (1) both of the compounds have the α branches whose dHvA frequencies are very close and their angular dependencies are similar, (2) both of the compounds have the β and γ branches whose dHvA frequencies are also very close, but in the case of $TmGa_3$ these branches exist in a narrower range of angles, and (3) instead of one lowest dHvA frequency branch δ for $LuGa_3$, there are several low frequency ones for $TmGa_3$.

IV. THEORY

The treatment of localized strongly correlated $4f$ electrons still presents a challenge to band structure theory. At the present time it is commonly believed[7–9] that within the local spin-density approximation (LSDA) a treatment of heavy rare-earth $4f$ states as bands is suitable for Gd and its compounds only, where the seven filled spin-up $4f$ states lie below, and the empty spin-down f states above the Fermi energy (E_F). But even for Gd, the calculated $4f$ bands appeared to be too close to E_F in comparison to experimental photoemission spectra (see Refs. 10–12). Also, the hybridization with other conduction electron states is apparently too large, raising the state density at E_F and leading to the unenhanced electronic specific heat coefficient which is larger than a measured value. The situation is far worse for other rare-earth metals since in spin-polarized calculations a spin shell is not filled and the $4f$ bands, which act as a sink for electrons, always cut the Fermi level, leading to absurd values of specific heat coefficients[7] and wrong $4f$ occupancies, close to the divalent (i.e., atomic) configuration.[12] The excellent analysis of this problem with ample references was given in Refs. 7–9. Also, the test band structure calculations for Gd and Er pnictides were carried out in Ref. 9 within LSDA, treating $4f$ states as bands, as well as the localized core states. By comparising the results of these calculations with a wealth of experimental data (including bulk and FS properties), the authors of Ref. 9 have obtained solid evidence that a strict band treatment for the $4f$ states is inadequate for heavy rare earths.

According to the photoemission data presented in Refs. 10–12, the $4f$ spectral density for Tm and Tm-based compounds was observed about 5 eV below E_F. Therefore, for the present purpose, which is mainly to describe the band structure for the trivalent ground state near E_F, it seems reasonable to treat $4f$ states as semilocalized core states, as

TABLE II. Comparison of the experimental dHvA results with theoretical ones for $LuGa_3$. λ is the mass enhancement factor.

		Experiment		Theoretical interpretation			
Branch	Orient.	F (10^6 Oe)	Mass [a]	Branch	F (10^6 Oe)	Mass [a]	λ
α	⟨100⟩	98.06	0.74	$R7$	89.8	0.38	0.95
α	⟨110⟩	94.6	0.73	$R7$	87.5	0.36	1.03
α	⟨111⟩	88.6	0.57	$R7$	82.3	0.36	0.58
β	⟨100⟩	41.3	0.63	$\Gamma 6$	46.35	0.48	0.31
β	⟨111⟩	35.6	0.53	$\Gamma 6$	38.64	0.39	0.36

[a]In units of free electron mass.

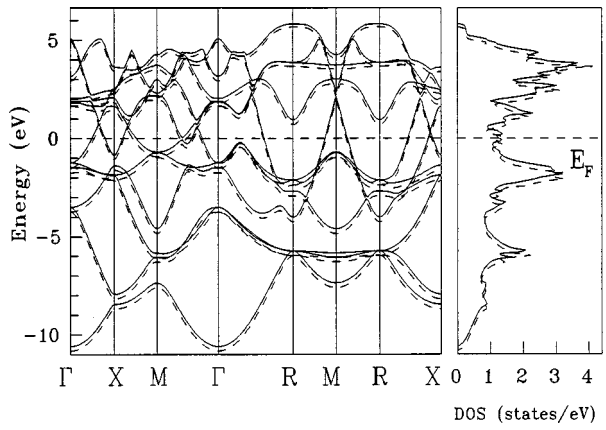

FIG. 7. Spin-polarized energy band structure along high symmetry planes calculated for $TmGa_3$ by LMTO method. The energy is measured from the Fermi energy E_F. Spin up — dashed curve, spin down — solid curve.

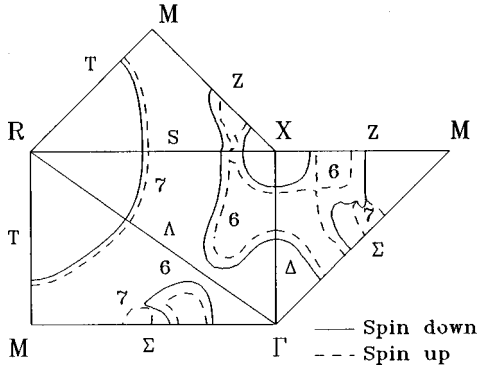

FIG. 8. Intersection of the Fermi surface for $TmGa_3$ with high symmetry planes for spin up and spin down. ''6'' and ''7'' — zone numbers.

is done in Refs. 7–9,13, and 14. The bulk and magnetic properties calculated within the same approach, as well as Fermi surfaces, of Tb (Ref. 8) and ErAs (Ref. 9) appeared to be in agreement with experimental data.

In the present paper the standard rare-earth model[7] is employed in the limit of the large Hubbard repulsion U within the *ab initio* LSDA scheme[15] for the exchange-correlation effects. The problem of handling localized f states of Tm was solved according to the method outlined in Refs. 13 and 14. Namely, the spin occupation numbers were fixed by applying the Russel-Saunders coupling scheme to the $4f$ shell. Therefore, the $4f$ states were not allowed to hybridize with conduction electrons. They were treated as spin-polarized outer-core wave functions, contributing to the total spin density, but not being a part of the band structure.

The self-consistent band structure calculations were carried out for $LuGa_3$ and also for the paramagnetic configuration phases of $TmGa_3$ by using the linear muffin-tin orbital method (LMTO) in the atomic sphere approximation (ASA) with combined corrections to ASA included.[16,17] In order to calculate Fermi surface orbits, the converged charge densities were obtained by including spin-orbit coupling at each variational step, as suggested in Refs. 7 and 8. In this case the spin is no longer a good quantum number, and it is not possible to evaluate the electronic structure for spin-up and spin-down bands separately.

Also, we have employed the standard approximation, which has been extremely successful for rare earths,[7] namely, to omit spin-orbit coupling in spin-polarized band structure calculations for $TmGa_3$. It provides a possibility to elucidate the role of the spin-orbit coupling, and also to present ''spin-up'' and ''spin-down'' bands for the field-induced ferromagnetic phase of $TmGa_3$, where the exchange splitting is much larger than spin-orbit splitting.

In the framework of the LSDA, the spin density of the $4f$ states polarizes the spin-up and spin-down conduction electron states through the local exchange interaction. The exchange split conduction electron states interact with the localized f states at other sites, appearing as the medium for the indirect f-f interaction.[14] The band structure was calculated on a uniform mesh of 455 points in the irreducible wedge of the cubic Brillouin zone for the experimental lattice constant value. The individual atomic radii of the components were consistently chosen following the general rule, proposed in Ref. 18.

We have checked results of the LMTO-ASA calculations by comparing with our own full potential LMTO calculations for selected high symmetry lines, and we found that the electronic structure and shape of FS are similar in the two types of calculations.

The results of the LMTO band structure calculations of $LuGa_3$ along the high symmetry lines in the Brillouin zone are shown in Fig. 5. The Fermi energy level crosses the sixth and seventh bands. An intersection of FS of the compound with the high symmetry planes of the Brillouin zone (Fig. 6) reveals a seventh-band electron FS centered at the R point and a sixth-band hole FS centered at Γ and X points. As seen from Table II, the agreement between results of FS calculations and experimental data is quite good. In agreement with the results of Ref. 8 for Gd and Tb, we have found that inclusion of spin-orbit coupling has a small effect on the calculated dHvA frequencies and cyclotron masses.

The results of the band structure calculations of the spin-polarized conduction band of $TmGa_3$ are shown in Fig. 7. The intersections of FS of the compound with the high symmetry planes of the Brillouin zone (Fig. 8) reveal the spin-up and spin-down seventh-band electron FS centered at the R point and the sixth-band hole FS centered at the Γ and X points, analogously to $LuGa_3$. As seen from Figs. 9 and 10, the electron paramagnetic FS of $TmGa_3$ is nearly spherical whereas the hole paramagnetic FS is the complicated multiply connected surface.

The densities of states $N(E)$ have been elaborated using the tetrahedron integration scheme on a fine energy mesh. They are displayed in Fig. 11. The main features of the density of states (DOS) for $TmGa_3$ can be described by two fairly broad peaks (bonding and antibonding states) arising due to hybridization of $5d$ states of Tm and Ga p states. The last one gives important contribution to the total DOS at the Fermi energy. Values of the DOS for $TmGa_3$ as well as for $LuGa_3$ are given in Table III.

V. DISCUSSION

The calculated angular dependence of FS extremal cross-section areas is presented in Fig. 2 together with the experi-

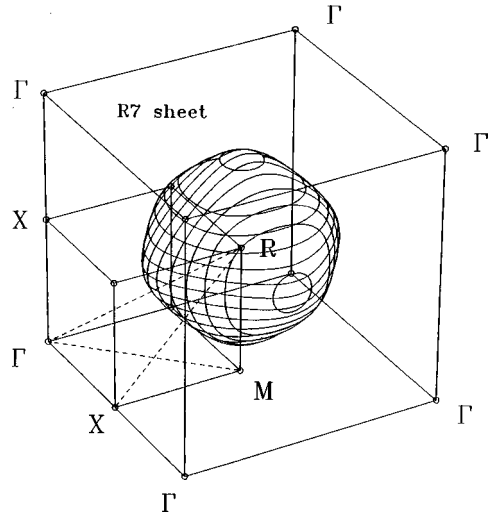

FIG. 9. Electron sheet of the Fermi surface in the seventh band for $TmGa_3$ in the paramagnetic phase.

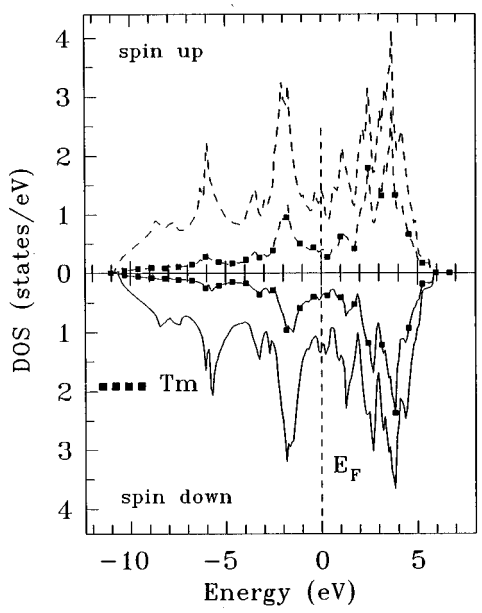

FIG. 11. Calculated total density of states for spin up (dashed curve) and spin down (solid curve). Filled square — partial density of states for Tm in $TmGa_3$.

mental data. The agreement is quite good (see also Table IV) for the extremal cross-section areas of the seventh-band electron FS (branch α) centered at the R point and the largest extremal cross-section area of the sixth-band hole FS centered at the Γ point (branch β). dHvA oscillations from various spin subbands of the branches α and β are not seen in the experiment. Also, the branch $X6$, expected from the spin-down FS sheet with frequency 7.95×10^6 Oe, is not observed.

In the range of the high dHvA frequencies (branches α and β) as well as the medium ones (branch γ) the spectra of $TmGa_3$ and $LuGa_3$ appeared to be very similar. In the low dHvA frequency range, instead of one branch (δ) for $LuGa_3$, several branches appear for $TmGa_3$.

One may assume that crystal potential in both compounds does not differ significantly. Therefore, the differences in the dHvA spectra can be attributed to the presence of an unfilled $4f$ shell in $TmGa_3$. As we have already mentioned in the Introduction, these differences come from two main sources: First, in the $4f$ spin-polarized state, from the splitting of the conduction band of $TmGa_3$ into ''spin-up'' and ''spin-down'' subbands; and second, from the magnetostriction effects due to the $\Gamma_5^{(1)}$ crystal field ground state of the $^3H_6$ multiplet of Tm^{3+} ion in the crystal field of $TmGa_3$. Unfortunately, one cannot attribute in an unambiguous way the differences in angular dependencies of dHvA frequencies in $TmGa_3$ and $LuGa_3$ either to the conduction band splitting and/or the magnetostriction.

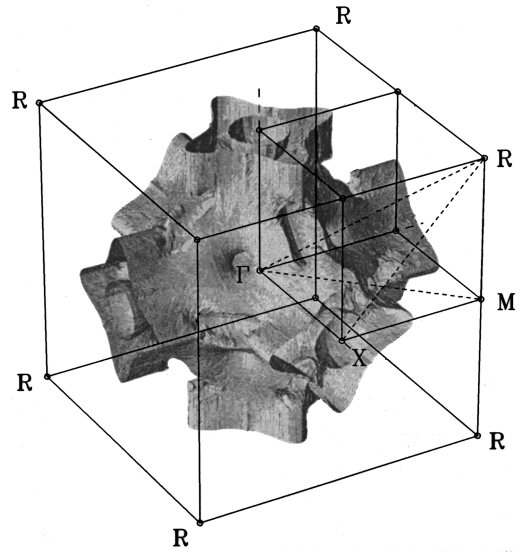

FIG. 10. Hole sheet of the Fermi surface in the sixth band for $TmGa_3$ in the paramagnetic phase. The Γ point is at the center.

Comparison of the calculated band masses with the effective cyclotron ones for the α and β orbits is given in Tables IV and II for $TmGa_3$ and $LuGa_3$, respectively. The mass enhancement factor λ, which is defined as the ratio of the cyclotron mass to the band mass $m_c=m_b(1+\lambda)$, in the case of $LuGa_3$ is a measure of the electron-phonon interaction whereas for $TmGa_3$ the λ factor also contains a contribution from the electron-magnetic excitations interaction.

Basically, the hybridization with the $4f$ states can also contribute to the larger masses observed in $TmGa_3$ than in $LuGa_3$ and affect the shape of the FS. Whereas the photoemission data give the occupied $4f$ states at 5 eV below E_F for pure Tm, the bremsstrahlung isochromat spectroscopy (BIS) excitation spectra indicate empty $4f$ levels at 1 eV above E_F (see Refs. 10–12). It should be emphasized, how-

TABLE III. Density of states at Fermi level and the unenhanced electronic specific heat coefficient γ_0 from the band structure calculations.

Compound	Spin	$N(E_F)$ (states/eV atom)	γ_0 (mJ/mol K^2)
$TmGa_3$	up	0.33	3.14
	down	0.32	3.09
$LuGa_3$		0.30	2.84

TABLE IV. Comparison of the experimental dHvA results with theoretical ones for $TmGa_3$. λ is the mass enhancement factor.

		Experiment		Theoretical interpretation			
Branch	Orient.	F (10^6 Oe)	Mass [a]	Branch	F (10^6 Oe)	Mass [a]	λ
α	$\langle 100\rangle$	98.70	1.2	$R7$	96.0 [b]	0.41	1.93
					87.7 [c]	0.40	
α	$\langle 110\rangle$	94.41	1.02	$R7$	92.8	0.38	1.68
					85.1	0.38	
α	$\langle 111\rangle$	87.28	0.77	$R7$	87.7	0.38	1.02
					79.9	0.37	
β	$\langle 100\rangle$	41.08	1.3	$\Gamma 6$	42.8	0.46	1.83
					34.0	0.40	
β	$\langle 111\rangle$	34.24	0.9	$\Gamma 6$	35.7	0.42	1.14
					28.1	0.34	

[a]In units of free electron mass.
[b]Spin up.
[c]Spin down.

ever, that this excited divalent configuration has only a distant relevance to our case of $TmGa_3$ studied in the trivalent ground state.

As was shown in Sec. IV, the hybridization effects are sufficiently overestimated within LSDA calculations. We believe that at the present stage even calculations within some modern LSDA+U scheme would not be of decisive importance, and more elaborate analysis is necessary to estimate a scale of the hybridization effects. In the case of a strong hybridization with $4f$ bands, a substantial reduction of the conduction band width in $TmGa_3$ would lead to a sizable and anisotropic effect on the cyclotron masses, but, at the same time, to remarkably different bulk properties in comparison to $LuGa_3$. By glancing at the experimental lattice parameters, which decrease slightly in a linear fashion in the series $ErGa_3$, $TmGa_3$, and $LuGa_3$ due to the lanthanide contraction, we can expect, however, that conduction band widths are very close in these compounds, and ''bare'' cyclotron masses should also be close.

The CF scheme in $TmGa_3$ gives the $\Gamma_5^{(1)}$ ground state with intrinsic magnetic and quadrupolar moments. It was shown in Refs. 19 and 20 that corresponding excitations contribute to the effective mass of the conduction electrons, and the effect appears to be large and magnetic field dependent. Obviously, this mechanism has to be taken into consideration in a future analysis of the experimentally observed differences between the cyclotron masses in $LuGa_3$ and $TmGa_3$.

One may expect that the presence of strong quadrupolar interactions increases cyclotron effective masses. It is well known[20] that the quadrupolar excitations do not occur in compounds with the cubic symmetry. They may appear, however, in $TmGa_3$ as coupled magnetic-quadrupolar excitations in applied magnetic field. Therefore, the enhancement factor λ, determined from comparison of the experimental cyclotron effective masses with the corresponding calculated ones, presumably contains a contribution from coupled magnetic-quadrupolar excitations.

As can be seen in Table II, in the nonmagnetic $LuGa_3$ compound the electron-phonon enhancement factor $\lambda_{e\text{-ph}}$ ranges from 0.3 (β branch) to 1 (α branch). These values are in agreement with the independent estimation of the averaged $\lambda_{e\text{-ph}}$, resulting from McMillan's relation[21] for superconducting $LuGa_3$ ($T_c = 2.35$ K): $\lambda_{e\text{-ph}} \simeq 0.6$. On the assumption that the values of $\lambda_{e\text{-ph}}$ in $TmGa_3$ are close to the corresponding ones in $LuGa_3$ (given as λ in Table II), and using values of λ presented in Table IV, one can estimate $\lambda_{e\text{-magnon}}$ factors for FS orbits in $TmGa_3$. According to our estimations, this factor appears to be more anisotropic than $\lambda_{e\text{-ph}}$, and varies within 0.5–1 and 0.8–1.5 for α and β orbits, respectively.

In conclusion, we can admit that more work is needed to elucidate the detailed nature of the large cyclotron masses observed in $TmGa_3$, and in particular, to evaluate the effects of coupling to magnetic-quadrupolar and CF excitations. Also the hybridization with $4f$ states should be taken into consideration as well in the framework of an *ab initio* rigorous version of LSDA+U or some other Hubbard-like approach. Obviously, these tasks go beyond the aim of the present paper, where we tried to reach a true LSDA limit within the standard rare-earth model, and remaining questions cannot be addressed by LSDA calculations.

ACKNOWLEDGMENTS

We are grateful to Professor J. Klamut and Professor I. V. Svechkarev for their kind support. This work has been performed within the research program of the Polish Committee for Scientific Research, KBN Nr 2 P302 091 06.

*Author to whom correspondence should be sent.

[1] V. B. Pluzhnikov, A. Czopnik, and I. V. Svechkarev, Physica B **212**, 375 (1995).
[2] A. Czopnik, Cz. Bazan, N. Iliev, B. Staliński, H. Mädge, and R. Pott, Physica B&C **130**, 262 (1985).
[3] P. Morin, M. Giraud, P. L. Regnault, E. Roudaut, and A. Czopnik, J. Magn. Magn. Mater. **66**, 345 (1987).
[4] P. Morin, M. Giraud, P. Burlet, and A. Czopnik, J. Magn. Magn. Mater. **68**, 107 (1987).
[5] P. Morin, J. Rouchy, M. Giraud, and A. Czopnik, J. Magn. Magn. Mater. **67**, 95 (1987).
[6] J. Pelleg, G. Kimmel, and D. Dayan, J. Less-Common Met. **81**, 33 (1981).
[7] M. S. S. Brooks and B. Johansson, in *Ferromagnetic Materials*, edited by K. H. J. Buschow (North-Holland, Amsterdam, 1993), Vol. 7, p. 139.
[8] R. Ahuja, S. Auluck, B. Johansson, and M. S. S. Brooks, Phys. Rev. B **50**, 5147 (1994).
[9] A. G. Petukhov, W. R. L. Lambrecht, and B. Segall, Phys. Rev. B **53**, 4324 (1996).
[10] J. F. Herbst and J. W. Wilkins, in *Handbook on the Physics and Chemistry of Rare Earths*, edited by K. A. Gschneidner, Jr., L. Eyring, and S. Hufner (North-Holland, Amsterdam, 1987), Vol. 10, p. 321.
[11] A. J. Freeman, B. I. Min, and M. R. Norman, in *Handbook on the Physics and Chemistry of Rare Earths*, edited by K. A. Gschneidner, Jr., L. Eyring, and S. Hufner (North-Holland, Amsterdam, 1987), Vol. 10, p. 321.
[12] B. I. Min, H. J. F. Jansen, T. Oguchi, and A. J. Freeman, J. Magn. Magn. Mater. **61**, 139 (1986).
[13] M. S. S. Brooks, L. Nordstrom, and B. Johanson, Physica B **172**, 95 (1991).
[14] G. E. Grechnev, A. S. Panfilov, I. V. Svechkarev, K. H. J. Buschow, and A. Czopnik, J. Alloys Compd. **226**, 107 (1995).
[15] U. von Barth and L. Hedin, J. Phys. C **5**, 1629 (1972).
[16] O. K. Andersen, Phys. Rev. B **12**, 3060 (1975).
[17] H. L. Skriver, *The LMTO Method* (Springer, Berlin, 1984).
[18] O. K. Andersen, O. Jepsen, and M. Sob, in *Electronic Band Structure and Its Applications*, edited by M. Yussouff (Springer, Berlin, 1987), p. 1.
[19] R. M. White and P. Fulde, Phys. Rev. Lett. **47**, 1540 (1981).
[20] P. Fulde and M. Loewenhaupt, Adv. Phys. **34**, 589 (1986).
[21] W. L. McMillan, Phys. Rev. **167**, 331 (1968).